Channel Estimation For The Multiuser Multipanel Massive Multiple Input Multiple Output System

Abbas Ghadiri
Azarbaijan Shahid Madani University
Mahmoud Atashbar (atashbar@azaruniv.ac.ir)
Azarbaijan Shahid Madani University https://orcid.org/0000-0003-3721-4128
M. Mohassel Feghhi
University of Tabriz

Research Article

Keywords: Channel estimation, Multipanel, Multiuser, Multiple input multiple output.

Posted Date: January 31st, 2022

DOI: https://doi.org/10.21203/rs.3.rs-1200572/v1

Channel Estimation for the Multiuser Multipanel Massive Multiple Input Multiple Output System

A. Ghadiri[1], M. Atashbar[1*], M. Mohassel Feghhi[2]

1. Department of Electrical Engineering, Azarbaijan Shahid Madani University, Tabriz, Iran

2. School of Electrical and Computer Engineering, University of Tabriz, Tabriz, Iran

[*]**Corresponding Author** : M. Atashbar, Department of Electrical Engineering, Azarbaijan Shahid Madani University, Tabriz, Iran, 53714-161, **Tel: +984131452550**, atashbar@azaruniv.ac.ir,

Abstract: By increasing the number of antennas, the size and weight of massive Multiple Input Multiple Output (MIMO) become much larger and heavier, respectively. To deal with these problems, the 3GPP standardization group captured the multipanel in New Radio communications. Channel estimation is needed for accurate uplink signal recovery and downlink precoding of massive MIMO. Due to the use of hybrid structure and the nonuniform distribution of the antenna arrays, the conventional channel estimation methods cannot be used in multipanel massive MIMO. In this paper, we propose the channel estimation for the millimeter-wave multipanel MIMO systems in multiuser environments, in which the channel estimation problem is transformed to an angular domain block sparse signal recovery problem. In the following, we solve the obtained sparse model using the proposed generalized block orthogonal matching pursuit method. Also, the proper pilot sequence is designed in the proposed method. Finally, we check the accuracy of the proposed estimation algorithm, which simulation results show the superior performance of the proposed method compared to that of the classic method.

KEYWORDS Channel estimation, Multipanel, Multiuser, Multiple input multiple output.

1 | INTRODUCTION

The demand for wireless communication throughput will always increase. Recently, millions of users simultaneously use different communication devices, and new users and their new needs are growing [1]. To cope with this problem, spectral efficiency should be increased. Therefore, the MIMO has been recently studied extensively as an effective technology and has been applied to many wireless standards [2]. This technology has been examined in recent years to focus on the multiuser MIMO systems, where a base station (BS) with multiple antennas simultaneously covers a range of multiple single-antenna users [3-4]. The next issue is the use of frequencies below 6 GHz. We know that the bands below 6 GHz for the cellular communication systems are being saturated, as of the limitations in access for the free spectrum (given the dedicated usage for each frequency band governed by the International Telecommunication Union). Hence, a solution to this problem is the use of free frequencies in the millimeter wave (mmWave) spectrum [5]. Although the mmWave brings us more bandwidth and higher capacity; however, the significantly larger loss is a drawback of this system [5]. To deal with this issue, a massive MIMO system is introduced in which many antennas are used to increase cell coverage [6]. This makes it possible to use effective and accurate algorithms for the beamforming and to be able to create a separate beam for each user. Therefore, in addition to counteracting the inherent fading in the mmWave, it can reduce the inter user

interference [7].

Meanwhile, to use many antennas at the BS, we will need much more power consumption, and also more implementation costs, since each antenna should be connected to a Radio Frequency (RF) chain. Thus, one of the significant issues is the number of RF chains in the massive MIMO systems, which poses many challenges to the practical implementation [5]. The use of hybrid array structures is a solution is proposed for reducing the RF chains[8-10]. In these structures, the number of RF chains is reduced compared to the conventional massive MIMO system, to reduce the power consumption and the structural complexity. Generally, these structures are divided into two categories: (1) the fully connected, and (2) the partially connected. In a fully connected structure, each RF chain is connected to all antennas, and in the partially connected structure, each RF chain is connected to a subset of the antennas [11]. Although the fully connected structure has better beamforming gain compared to the partially connected structure; however, it requires a lot of phase shifters to connect each RF chain to all antennas, which means more power consumption. Consequently, the partially connected structure provides lower power consumption and weaker beamforming gain. In this paper, we consider the partially connected structure as the desired structure.

On the other hand, in the implementation of an array, by increasing the number of antennas, the size and weight of massive MIMO become much larger and heavier respectively, which leads to many problems such as [12]; difficulty in installing the massive MIMO on the existing antenna poles, difficulty moving the array, increasing the complexity and cost of massive MIMO maintenance, etc. to deal with these problems, 3GPP standardization group captured the multipanel in New Radio (NR) communications [13-14]. To more increase the multiplexing gain within one panel, the fully connected with more than one RF chain can be used in an advanced multipanel array [15]. Also, the multipanel array can be used in single cell and multi cell scenarios [16]. A multipanel system can reduce the mutual coupling effect on each panel and create more favorable beamforming [17,18]. Moreover, by eliminating the antenna in package (AIP) structures, more desirable performance is provided compared to that of the other structures (in terms of configuration and maintenance) [17]. Uniform multipanel array (UMPA) and Nonuniform mulipanel array (NUMPA) are two antenna structures that can be used in the multipanel massive MIMO. As seen in Fig. 1, in UMPA, the spacing between two adjacent antenna elements from different antenna panels is the same as the spacing between two antenna elements in the same antenna panel. While in the NUMPA the spacing between two adjacent antennas from different panels is larger than the spacing between antennas in the same panel [17].

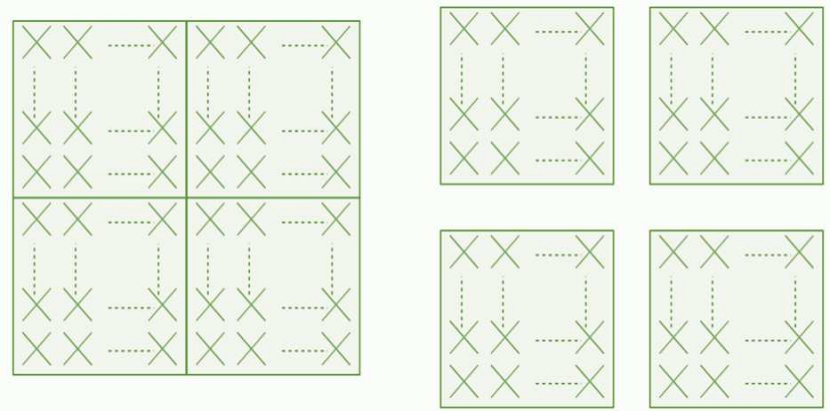

a. Uniform b. Nonuniform

Fig. 1 Example of Uniform and Nonuniform multipanel array

Another important issue to be considered is channel estimation. Obtaining accurate channel state information (CSI) can help the receiver provide better recovery for the signal sent into the wireless environment [19-21]. Due to hybrid structure and nonuniform antenna array, existing channel estimation cannot be directly applied to multipanel massive MIMO [22]. There are a few kinds of research on this issue. In [22], the channel estimation and hybrid precoding are investigated for multipanel massive MIMO, in which the uplink channel is estimated using sparse modeling of the mmWave Massive MIMO channel in the angular domain to overcome in pilot overhead problem. The same method is used in [23], in which the orthogonal projection method is introduced for solving the obtained sparse model. Both these methods assume that only one user is presented in the channel estimation stage.

In this paper, we propose channel estimation of multipanel massive MIMO in the multiuser scenario. The proposed method is an extension of the method presented in [23]

to the multiuser case. In the proposed method, using the angular domain sparsity feature of mmWave massive MIMO channel, the multiuser channel estimation problem is formed as a linear sparse model, in which unknown sparse vector has block sparse property so that user related elements are arranged sequentially. By solving this sparse problem, the channels of all users are estimated, simultaneously, where the generalized block Orthogonal Matching Pursuit (OMP) method is proposed for solving this sparse model. Also, the pilot design of the proposed method is investigated.

The rest of this paper is organized as follows. In the next section, the system modeling is presented. In section 3, the proposed method is introduced, and the simulation results are then presented in section 4, finally, the paper is concluded in section 5.

2 | SYSTEM MODELING

We consider a system in the uplink with a cell consisting of a BS with N_p panels, where each panel is connected to only one RF chain. Also, we consider N_a antennas in each panel; so, we need N_a phase shifter. Thus, the total number of antennas is $N_t = N_p N_a$. Also, we assume that there are L users in the cell, each has one antenna. In this case, the existing channel matrix between the n_p-th antenna panel and the l-th user is as follows [23]:

$$\boldsymbol{h}_{n_p,l} = \sum_{k=1}^{K} \alpha_{k,n_p,l} \boldsymbol{a}_b(\phi_{k,l}) \tag{1}$$

where, the $\phi_{k,l}$ is the angle of arrival (AoA) of the l-th user' signal in the k-th path, respectively, K is the number of paths, $\boldsymbol{a}_b(\phi_{k,l})$ is the steering vector at the BS, which is expressed as:

$$\boldsymbol{a}_b(\phi_{k,l}) = \left[1, e^{j\pi 1\phi_{k,l}}, \cdots, e^{j\pi(N_a-1)\phi_{k,l}}\right]^T \tag{2}$$

Also, $\alpha_{k,n_p,l} \triangleq \alpha_{k,l} e^{j\left(\pi\frac{2\tau_{n_p}}{\lambda}\zeta_{k,l}+\vartheta_{np}\right)}$ is the complex coefficient of the k-th path between the n_p-th panel and the l-th user, λ is the wavelength, τ_{np} is the distance between the reference panel and the n_p-th panel, ϑ_{np} is the phase ambiguity among the different panels, and $\zeta_{k,l} \in (-1,1]$ is the cosine of the AoA on the BS corresponding to the k-th path. By selecting the first panel as the reference panel, we have $\tau_1 = 0$, and assuming the same distance between different panels, we have $\tau_a = \frac{\lambda}{2}$. Now we can write (1) in the matrix form as:

$$\boldsymbol{h}_{n_p,l} = \boldsymbol{A}_{b,l}\boldsymbol{\beta}_{n_p,l} \tag{3}$$

where,

$$\boldsymbol{A_{b,l}} = [\boldsymbol{a}_b(\phi_{1,l}) \quad \boldsymbol{a}_b(\phi_{2,:}) \quad \ldots \quad \boldsymbol{a}_b(\phi_{K,l})] \tag{4}$$

$$\boldsymbol{\beta}_{n_p,l} = [\alpha_{1,n_p,l} \quad \alpha_{2,n_p,l} \quad \ldots \quad \alpha_{K,n_p,l}]^T \tag{5}$$

In the uplink transmitting of the multipanel massive MIMO, it is assumed that a part of the receiver's beamforming process is done in the analog form; since the number of RF chains is limited. Combining the signals of a panel with the coefficients corresponding to the analog phase shifters introduces a scalar value in an RF chain. Hence, from a mathematical view, the output of the RF chain connected to the n_p-th panel is equivalent to the product of the received signal vector (in the n_p-th panel antennas) at vector $\mathbf{m}_{n_p}$, which $\mathbf{m}_{n_p}$ is the phase shifter vector for N_a antennas at the n_p-th panel, and it is expressed as [23]:

$$\boldsymbol{m}_{n_p} = \frac{1}{\sqrt{N_a}}\left(e^{j\pi\varrho_{1,n_p}}, e^{j\pi\varrho_{2,n_p}}, \cdots, e^{j\pi\varrho_{N_a,n_p}}\right)^T \tag{6}$$

where ϱ_{n_a,n_p} is an analog phase shifter from the n_a-th antenna at the n_p-th panel. The value of this phase shifter is selected randomly with the uniform distribution in [0,2π). If s_l be the pilot signal sent by the l-th user, the received signal in the output of the n_p-th panel can be described as:

$$\bar{y}_{n_p} = \boldsymbol{m}_{\boldsymbol{n_p}}^{\boldsymbol{T}} \sum_{\boldsymbol{l=1}}^{\boldsymbol{L}} \boldsymbol{h}_{\boldsymbol{n_p},\boldsymbol{l}} s_l + \boldsymbol{m}_{\boldsymbol{n_p}}^{\boldsymbol{T}} \boldsymbol{w} \tag{7}$$

where $\boldsymbol{w} \sim \mathcal{CN}\left(\mathbf{0}_{N_t \times 1}, \sigma_w^2 \boldsymbol{I}_{N_a}\right)$ be the noise vector in the antennas of n_p-th panel. By combining the output signals of all panels, we have

$$\bar{\boldsymbol{y}} = \boldsymbol{M} \sum_{l=1}^{L} \boldsymbol{h}_l s_l + \boldsymbol{n} \tag{8}$$

where $\boldsymbol{h}_l \in \mathbb{C}^{N_a \times 1}$ is the channel vector between the BS and the l-th user as $\boldsymbol{h}_l = \left[\boldsymbol{h}_{1,l}^T, \boldsymbol{h}_{2,l}^T, \cdots, \boldsymbol{h}_{N_p,l}^T\right]^T$, $\boldsymbol{M} \in \mathbb{C}^{N_p \times N_t}$ is the combining matrix used at the BS, which is represented as:

$$\boldsymbol{M} = blkdiag(\boldsymbol{m}_1^T, \boldsymbol{m}_2^T, \ldots, \boldsymbol{m}_{N_p}^T) \tag{9}$$

where $blkdiag(.)$ defines the block diagonalization [24], and $\boldsymbol{n} \triangleq \boldsymbol{M}\boldsymbol{w}$ represents the noise vector at the output of the RF chains.

In the multiuser massive MIMO channel estimation, we estimate channel matrices $\boldsymbol{h}_1, \boldsymbol{h}_2, .., \boldsymbol{h}_L$ in (8), in which it is assumed that $\bar{\boldsymbol{y}}, \boldsymbol{M},$ and $\boldsymbol{s}_l$ are known matrices or vectors. According to (8), we have a system of linear equations, where the number of unknown parameters is $N_p N_a L$, and the number of equations is N_p. As a result, sending the pilot signal at only one symbol is impossible for solving this problem. To make the problem to be solvable, the pilot sequence must be sent in many symbols (at least $N_a L$ symbols), and by combining the obtained information, the channel matrices will be estimated. Thus, for accurate estimation, we need to assign many symbols to the pilot symbols. This leads to the pilot overhead problem. To deal with this problem. in this paper, we use compressed sensing theory for estimating the channel matrices of all users simultaneously.

3 | PROPOSED METHOD

In this section, we propose the compressed sensing based modeling of the multiuser multipanel channel estimation of the massive MIMO system and the method for solving it.

3.1 | Proposed sparse modeling

In practice, the number of paths associated with each user (K) is very smaller than the number of BS antennas, thus we can assume that the channel vector is sparse in the angular domain, and $\boldsymbol{h}_{n_p,l}$ can be sparsely represented as

$$\boldsymbol{h}_{n_p,l} = \boldsymbol{A}_{bos} \boldsymbol{b}_{n_p,l} \tag{10}$$

where

$$\boldsymbol{b}_{n_p,l} = \left[\xi_{1,n_p,l} \quad \xi_{2,n_p,l} \quad \cdots \quad \xi_{N_a K_s,n_p,l}\right]^T \tag{11}$$

$$\boldsymbol{A}_{bos} = [\boldsymbol{a}(\varphi_1) \quad \boldsymbol{a}(\varphi_2) \quad \ldots \quad \boldsymbol{a}(\varphi_{N_a K_s})] \tag{12}$$

, $\varphi_i = \left(-1 + \frac{2i}{N_a K_s}\right)\pi$ is the i-th oversample angle, and K_s is the oversampling factor that is selected so that, $\phi_{k,l}$ is approximately equal to one of oversample angle values $\varphi_i, i = 1,2,..,N_a K_s$. In this case, $\boldsymbol{b}_{n_p,l}$ is $N_a K_s \times 1$ sparse vector with K nonzero elements associated with $\phi_{1,l}, \phi_{2,l}, .. \phi_{K,l}$, where if $\varphi_{i_k} = \phi_{k,l}$, then $\xi_{i_k,n_p,l} = \alpha_{k,n_p,l}$. If we consider support set of $\boldsymbol{b}_{n_p,l}$ as $\mathfrak{H}_{n_p,l} = supp\left\{\boldsymbol{b}_{n_p,l}\right\} \triangleq \{i: \left|\xi_{i,n_p,l}\right| > 0\}$, we can assume that $\mathfrak{H}_{1,l} = \mathfrak{H}_{2,l} = \cdots = \mathfrak{H}_{N_p,l}$, which

indicates that the support set of $\boldsymbol{b}_{n_p,l}$ associated with different antenna panels are equal. Since the distance between adjacent antennas in the BS antenna array is very smaller than the distance between BS and users, we can assume that the signal is received to all panels with the same AOA, which leads to similar sparsity pattern for all panels. In this case, if we represent the pilot sent by the *l*-th user at the *n*-th symbol by $\boldsymbol{s}_l(n)$, the received signal of the n_p-th panel at the output of the RF chain is equal to:

$$\tilde{y}_{n_p}(n) = \boldsymbol{m}_{n_p}^T \sum_{l=1}^{L} \boldsymbol{A}_{bos} \boldsymbol{b}_{n_p,l} s_l(n) + n_{n_p}(n) \tag{13}$$

Now, by combining the signals at the output of the RF chains, we have:

$$\tilde{\boldsymbol{y}}(n) = \boldsymbol{M}_a \sum_{l=1}^{L} \boldsymbol{b}_l s_l(n) + \boldsymbol{n}(n) \tag{14}$$

where $\tilde{\boldsymbol{y}}(n) = [\tilde{y}_1(n), \tilde{y}_2(n), \ldots, \tilde{y}_{N_p}(n)]^T$ and $\boldsymbol{n}(n) = [n_1(n), n_2(n), \ldots, n_{N_p}(n)]^T$ are the received signal and the noise vector from all RF chains, respectively, $\boldsymbol{M}_a = \boldsymbol{M}\boldsymbol{A}_{bos}$, and

$$\begin{aligned} \boldsymbol{b}_l &= [\boldsymbol{b}_{1,l}^T, \boldsymbol{b}_{2,l}^T, \ldots, \boldsymbol{b}_{N_p,l}^T]^T \\ &= [\xi_{1,1,l}, \ldots, \xi_{N_a K_s,1,l}, \xi_{1,2,l}, \ldots, \xi_{N_a K_s,2,l}, \ldots, \xi_{1,N_p,l}, \ldots, \xi_{N_a K_s,N_p,l}]^T \end{aligned} \tag{15}$$

Thus, the $\boldsymbol{b}_l$ is a $N_a K_s N_p \times 1$ sparse vector with KN_p nonzero elements. Since all of $\boldsymbol{b}_{1,l}, \boldsymbol{b}_{2,l}, \ldots, and\ \boldsymbol{b}_{N_p,l}$ have a similar support set, we rearrange the elements of $\boldsymbol{b}_l$ so that, the nonzero elements associated with all panels become adjacent, which leads to a block sparse matrix. In other words, the vector $\boldsymbol{b}_l$ is rewritten as the vector $\boldsymbol{c}_l$ as

$$\boldsymbol{c}_l = [\xi_{1,1,l}, \xi_{1,2,l}, \ldots, \xi_{1,N_p,l}, \xi_{2,1,l}, \xi_{2,2,l}, \ldots, \xi_{2,N_p,l}, \ldots, \xi_{N_a K_s,1,l}, \xi_{N_a K_s,2,l}, \ldots, \xi_{N_a K_s,N_p,l}]^T \tag{16}$$

which is written at the bottom of the page. In this case, according to (14), the matrix $\boldsymbol{M}_a$ should be changed to the matrix $\boldsymbol{M}_c$ as. (17).

$$\boldsymbol{M}_c = \begin{bmatrix} \boldsymbol{m}_1^T \boldsymbol{a}(\phi_1) & \ldots & \boldsymbol{m}_{N_p}^T \boldsymbol{a}(\phi_1) & 0 & \cdots & 0 & 0 & \cdots & 0 \\ 0 & \ldots & 0 & \boldsymbol{m}_1^T \boldsymbol{a}(\phi_2) & \cdots & \boldsymbol{m}_{N_p}^T \boldsymbol{a}(\phi_2) & 0 & \cdots & 0 \\ \vdots & \vdots & \vdots & \vdots & \vdots & \vdots & \vdots & \vdots & \vdots \\ 0 & \cdots & 0 & 0 & \cdots & 0 & \boldsymbol{m}_1^T \boldsymbol{a}(\phi_{N_a K_s}) & \cdots & \boldsymbol{m}_{N_p}^T \boldsymbol{a}(\phi_{N_a K_s}) \end{bmatrix} \tag{17}$$

Hence, (14) is rewritten as:

$$\tilde{\boldsymbol{y}}(n) = \boldsymbol{M}_c \sum_{l=1}^{L} \boldsymbol{c}_l s_l(n) + \tilde{\boldsymbol{n}}(n) \tag{18}$$

Now, by combining the pilot sequence of the different users, (18) is represented as:

$$\tilde{\boldsymbol{y}}(n) = \boldsymbol{M}_c \boldsymbol{C} \boldsymbol{s}(n) + \tilde{\boldsymbol{n}}(n) \tag{19}$$

where, $\boldsymbol{C} = [\boldsymbol{c}_1 \quad \boldsymbol{c}_2 \quad \cdots \quad \boldsymbol{c}_L]$ and $\boldsymbol{s}(n) = [s_1(n), s_2(n), \ldots, s_L(n)]^T$. Now, if the transmitted pilot sequences are carried in the N_ϕ symbols, by combining correspond received N_ϕ symbols in the column of matrix $\tilde{\boldsymbol{Y}}$, we have

$$\tilde{\boldsymbol{Y}} = \boldsymbol{M}_a \boldsymbol{C} \boldsymbol{S} + \tilde{\boldsymbol{N}} \tag{20}$$

where $\tilde{\boldsymbol{Y}} = [\tilde{\boldsymbol{y}}(1), \tilde{\boldsymbol{y}}(2), \ldots \tilde{\boldsymbol{y}}(N_\phi)]$, $\tilde{\boldsymbol{N}} = [\tilde{\boldsymbol{n}}(1), \tilde{\boldsymbol{n}}(2), \ldots \tilde{\boldsymbol{n}}(N_\phi)]$, and $\boldsymbol{S} = [\boldsymbol{s}(1), \boldsymbol{s}(2), \ldots, \boldsymbol{s}(N_\phi)]$.

By using the matrix relations presented at [12], we can change (20) to the vector form as follows:

$$\boldsymbol{y} = \boldsymbol{D}\boldsymbol{c} + \boldsymbol{n}_v \tag{21}$$

Where $\boldsymbol{n}_v = vec(\boldsymbol{N})$, $\boldsymbol{y} = vec(\tilde{\boldsymbol{Y}})$ contains the output values of the BS array RF chains in N_ϕ symbols, $\boldsymbol{D} = \boldsymbol{S}^T \otimes \boldsymbol{M}_c$ is calculated by using the pilot sequence, analog beamforming values, and oversampling angles. Thus, the values of $\boldsymbol{y}$ and $\boldsymbol{D}$ are known. On the other hand, $\boldsymbol{c} = vec(\boldsymbol{C}) = [\boldsymbol{c}_1^T \quad \boldsymbol{c}_2^T \quad \cdots \quad \boldsymbol{c}_L^T]^T$ is

a $N_p N_a K_s L \times 1$ unknown vector that the l-th block of this vector corresponds to the l-th user. Furthermore, $\boldsymbol{c}$ has a block sparsity nature with nonzero elements corresponding to actual AOA angles of paths, thus, by estimating $\boldsymbol{c}$ based on (21), the channels of all users are obtained.

3.2 | Proposed generalized block OMP method

In this section, we investigate a mechanism to recover the $\boldsymbol{c}$ in (21), for this purpose, the generalized version of the block OMP method is used. In (21), $\boldsymbol{c}$ is an $N_p N_a K_s L \times 1$ vector that is reconstructed by concatenation of $J = N_a K_s L$ blocks which each block has N_p elements as:

$$\boldsymbol{c} = \left[\boldsymbol{c}^T[1] \;\; \boldsymbol{c}^T[2] \;\; \ldots \;\; \boldsymbol{c}^T[J]\right]^{\boldsymbol{T}} \tag{22}$$

which the elements are indicated in (23).

$$\begin{aligned}
&\boldsymbol{c}[1] = [\xi_{1,1,1}, \xi_{1,2,1}, \ldots, \xi_{1,N_p,1}]^T \quad , \quad \ldots \quad , \quad \boldsymbol{c}[N_a K_s] = [\xi_{N_a K_s,1,1}, \xi_{N_a K_s,2,1}, \ldots, \xi_{N_a K_s,N_p,1}]^T \\
&\boldsymbol{c}[N_a K_s + 1] = [\xi_{1,1,2}, \xi_{1,2,2}, \ldots, \xi_{1,N_p,2}]^T \quad , \ldots \quad , \quad \boldsymbol{c}[2N_a K_s] = [\xi_{N_a K_s,1,2}, \xi_{N_a K_s,2,2}, \ldots, \xi_{N_a K_s,N_p,2}]^T \\
&\qquad\qquad\qquad\qquad\qquad\qquad \vdots \\
&\boldsymbol{c}[(L-1)N_a K_s + 1] = [\xi_{1,1,L}, \xi_{1,2,L}, \ldots, \xi_{1,N_p,L}]^T , \ldots , \boldsymbol{c}[LN_a K_s] = [\xi_{N_a K_s,1,L}, \xi_{N_a K_s,2,L}, \ldots, \xi_{N_a K_s,N_p,L}]^T
\end{aligned} \tag{23}$$

According to the block sparse nature of $\boldsymbol{c}$, only LK of the J blocks can have nonzero elements. By finding the location and values of these blocks, the channels associated with all users are estimated. To use the block sparse nature of the $\boldsymbol{c}$ to solve (21), in each step of the OMP algorithm [25], the energy of each block must be calculated, and the location of the blocks with the maximum energy is considered as an estimate of the location of the nonzero blocks. The stages of the algorithm are shown in algorithm 1.

Alghoritm1: Extended block OMP algorithm

1: **Initialize**: $\boldsymbol{r} = \boldsymbol{y}$, $\hat{\boldsymbol{c}} = \boldsymbol{0}_{JN_p \times 1}$, $\boldsymbol{Q} = \boldsymbol{0}_{J \times 1}$ (all zero vectors), $\hat{J} = \emptyset$

2: **Compute**: $\boldsymbol{p} \leftarrow \boldsymbol{D}^H \boldsymbol{r}$

3: **Assign**: $Q_j = \sqrt{\sum_{i=1}^{Np} \left| p_{(j-1)N_p + i} \right|^2}$ for $j = 1,2,\ldots,J$

4: **Count**: $j^* = arg\ \underset{j}{max}\ [\boldsymbol{Q}]$, $\hat{\jmath} = \{(j^* - 1)N_p + 1, \ldots, j^* N_p\}$

5: **Store**: $sort(\hat{J} \cup \hat{\jmath}) \rightarrow \hat{J}$

6: **Evaluate**: $\underset{\boldsymbol{x}}{argmin} \|\boldsymbol{y} - \boldsymbol{D}_{\hat{\jmath}} \boldsymbol{x}\|_2 \rightarrow \boldsymbol{x}_t$, where $\boldsymbol{D}_{\hat{\jmath}}$ is the subset of matrix $\boldsymbol{D}$ and $\hat{J}$ is an index of columns of the matrix $\boldsymbol{D}$.

7: **Update**: $\boldsymbol{r} = \boldsymbol{y} - \boldsymbol{D}_{\hat{\jmath}} \boldsymbol{x}_{\boldsymbol{t}}$

8: **Returns to step 2**. The algorithm is stopped if $\hat{J}$ has $\lceil N_p KLa \rceil$ elements.

9. **Compute**: $\hat{\boldsymbol{c}}_{\hat{\jmath}} = \left(\boldsymbol{D}_{\hat{\jmath}}^H \boldsymbol{D}_{\hat{\jmath}}\right)^{-1} \boldsymbol{D}_{\hat{\jmath}}^H \boldsymbol{y}$

10: **Assign:** $Q'_j = \sqrt{\sum_{i=1}^{Np} \left| c_{(j-1)N_p + i} \right|^2}$ for $j = 1,2,\ldots,J$.

11. **Final estimation**: Set zero the values of $\hat{\boldsymbol{c}}[j_1]$, $\hat{\boldsymbol{c}}[j_2], \ldots, \hat{\boldsymbol{c}}[j_{\lceil KLa \rceil - KL}]$, where j_k is index of the k-th smallest value in $\boldsymbol{Q}'$.

In the following, we explain each step of the block OMP algorithm, named algorithm 1. After a selection of the initial values in step 1, we calculate the multiplication of the

matrix $\mathbf{D}$ and the residual vector $\mathbf{r}$ in step 2. In step 3, we compute the matrix $\boldsymbol{Q}$, which its j-th element is the energy of j-th blocks of vector $\boldsymbol{p}$, then the index of a block with the largest energy (j^*) is calculated in step 4, and corresponding indices in $\boldsymbol{p}$ is named as $\hat{\jmath}$. This finally leads to the detection of the location of the active elements. The new active elements' location is added with that of the previous in stage 5. In the next stage, the nonzero elements of sparse vector $\boldsymbol{x}$ are estimated with LS criterion by using the subset of $\boldsymbol{D}$ associated with the active elements' locations. Finally, at step 7, the residual vector is updated by removing the portion of the selected columns in the previous steps.

These stages are repeated until $\hat{\jmath}$ has $[KLa]$ elements, where $a > 1$ is a constant and [.] denotes the floor function. In this case, $\hat{\jmath}$ indicates the location of $[KLa]$ nonzero elements of $\hat{\boldsymbol{c}}$, thus the value of these nonzero elements can be estimated using LS criterion as done in stage 9. Since we have KL nonzero N_p-length block in vector $\boldsymbol{c}$, and $[N_p KLa] \geq N_p KL$, we need to remove additional nonzero blocks of $\hat{\boldsymbol{c}}$. For this purpose, the energy of each N_p-length block of $\hat{\boldsymbol{c}}$ is estimated in stage10 and KL blocks with the largest energy are selected as the final nonzero blocks, finally, the values of other blocks are set to zero in stage 11.

3.3 | Pilot sequence design

For estimating the channels between antennas of BS and all users, each user must transmit an individual pilot sequence. To reduce the pilot overhead problem, we assume that all users simultaneously transmit their pilot sequences and all channels are estimated using a compressive sensing theory. In this section, we discuss the constrain of the pilot sequences of each user and analog phase shifter values to achieve the accurate estimation of the multipanel MIMO channels based on the block sparsity algorithm investigated in the previous section.

For solving a sparse problem using compressive sensing theory, mutual coherence has an important role in the accuracy of estimation. This parameter defines as follow [26]

$$\mu_D = \underset{i_1 \neq i_2}{max} \frac{|\boldsymbol{D}_{i_1}^H \boldsymbol{D}_{i_2}|}{\|\boldsymbol{D}_{i_1}\|_2 \|\boldsymbol{D}_{i_2}\|_2} \tag{24}$$

In which $\boldsymbol{D}_i$ indicates the i-th column of $\boldsymbol{D}$. According to (24) we have $0 \leq \mu_D \leq 1$. For the small mutual coherence, the compressed sensing algorithms have better performance. In the case that the column of $\boldsymbol{D}$ has strong similarity, the value of mutual coherence is large which leads to low accuracy estimation.

Thus, to achieve high accuracy channel estimation, we need to have a small value for μ_D. According to $\boldsymbol{D} = \boldsymbol{S}^T \otimes \boldsymbol{M}_c$, the Kronecker multiplication between the pilot sequences matrix and the measurement matrix creates a challenge to achieve the minimum value of the mutual coherence parameter. To better understand this issue, we display $\boldsymbol{D}$ as follow:

$$\boldsymbol{D} = \begin{bmatrix} \mathrm{s}_1(1)\mathbf{M}_\mathrm{c} & \mathrm{s}_2(1)\mathbf{M}_\mathrm{c} & \cdots & \mathrm{s}_\mathrm{L}(1)\mathbf{M}_\mathrm{c} \\ \mathrm{s}_1(2)\mathbf{M}_\mathrm{c} & \mathrm{s}_2(2)\mathbf{M}_\mathrm{c} & \cdots & \mathrm{s}_\mathrm{L}(2)\mathbf{M}_\mathrm{c} \\ \vdots & \vdots & \ddots & \vdots \\ \mathrm{s}_1(\mathrm{N}_\varphi)\mathbf{M}_\mathrm{c} & \mathrm{s}_2(\mathrm{N}_\varphi)\mathbf{M}_\mathrm{c} & \cdots & \mathrm{s}_\mathrm{L}(\mathrm{N}_\varphi)\mathbf{M}_\mathrm{c} \end{bmatrix} \tag{25}$$

As you can see, the values of the pilot sequence play a key role in differentiating some columns of $\boldsymbol{D}$. For example, according to (17) and (25), the pilot sequences of 1-th and 2-th user determinate the distinction between the 1-th and $(N_a K_s N_p + 1)$-th columns of $\boldsymbol{D}$. Therefore, to minimize the mutual coherence, addition to that the pilot sequence have different values in different symbols, each user must have a unique pilot sequence. Also, to ensure unit power constraint for transmitted pilot sequence, we assume that each element of the pilot has unit magnitude. To meet these constraints, we choose the n-th pilot of l-th user as $\mathrm{s_l(n)} = e^{j\theta_{ln}}$, in which θ_{ln} is a random variable with uniform distribution over $[0, 2\pi]$.

On the other hand, according to (17) and (25), the mutual coherence of some adjacent column of $\boldsymbol{D}$ (such as 1-th to N_p-th or $(N_p + 1)$-th to $2N_p$-th columns) depends on the values of analog beamforming coefficients. If the phase shifter vectors associated with all panels or all training symbols are equal, a large value is obtained for the mutual coherence of these adjacent columns. Thus, to deal with this problem, we select different values for the phase shifter vectors of all panels and all training symbols.

4 | SIMULATION RESULTS

In this section, our goal is to evaluate the performance of the proposed algorithm in the multiuser scenario, using the Normalized Mean Square Error (NMSE) and the Bit Error Rate (BER) metrics, and compare them with the results obtained by the classical method. The classical method refers to the algorithm presented in [23] is proposed in the

single-user scenario. To create the possibility to use the results of this algorithm for comparison with the multiuser scenario, we assume that each user sends a pilot sequence in certain symbols, individually, then its channel is estimated using the method of [23]. However, in the proposed method, we simultaneously estimate the channel matrix of all users and do not discriminate among the users in the estimation process. In the figures of simulation results, we legend the results obtained from the proposed algorithm as "proposed", and the results obtained from the classical algorithm as "classic". Also, these results have been calculated using computer simulations in the MATLAB environment based on the Monte Carlo technique, averaging over the 5000 trials for NMSE criterion and the 50000 trials for BER criterion.

In the simulations, the number of active paths between each user and the BS has been selected as k =2, which indicates a very lower number of paths. The reason is the high fading of the signals from the different paths, due to the inherent losses of the mmWave signals. The number of antennas within each panel is 32, and the number of panels is 4, which leads to the total number of used antennas be 128.

4.1 | Comparing the methods via NMSE

The first criterion for comparing different estimation methods is NMSE which is defined as:

$$NMSE = \frac{1}{L}\sum_{l=1}^{L} \frac{E\left\{\left\|\hat{\boldsymbol{h}}_l - \boldsymbol{h}_l\right\|^2\right\}}{E\{\|\boldsymbol{h}\|^2\}} \tag{26}$$

in which $\boldsymbol{h}_l$ and $\hat{\boldsymbol{h}}_l$ are the actual and estimated channel vector of l-th user. In the first simulation, we select L=2, $Ks = 8$, and $N\varphi = 8$, and compare the NMSE versus SNR for the proposed and the classical algorithms. The results are shown in Fig. 2, indicate that as the SNR increases, the NMSE decreases to an acceptable level, as expected. At low SNRs, both methods have a relatively similar performance; however, by increasing the SNR, the proposed method presents more favorable results. For example, at SNR=5 dB, the results obtained for the proposed algorithm and the classical algorithm are 0.2247 and 0.2468, respectively. However, at SNR=35 dB, the values obtained for the proposed algorithm and the classical algorithm are 0.0991 and 0.1365, respectively. In addition, we see an error floor in the classical algorithm at SNR=30 dB, and the NMSE performance no longer improves by increasing the SNR. While in the proposed algorithm, there is no such an error floor, and the NMSE performance is improving by increasing the SNR.

Therefore, to investigate the effect of pilot sequence length, we assume $N\varphi = 6$ in the second simulation. In this simulation, we still have $Ks = 8$, and the NMSE performances versus the SNR are provided. The results obtained in Fig 3 indicate that by decreasing the length of the pilot sequence, the channel estimation performance decreases to some extent. This is because the measurement matrix **M** finds fewer rows than the case in Fig 2, which increases the error compared to the case with $N\varphi = 8$. Therefore, the channel estimation accuracy is reduced in Fig 3 compared to that of Fig 2. This reduction in accuracy is lower in the proposed algorithm than the classic algorithm. For example, at SNR=5 dB, the NMSE obtained for the proposed and classic methods are 0.2996 and 0.3494, respectively, and for SNR=35 dB, it is 0.1733 and 0.2472, respectively. By comparing these results with that obtained in the case $N\varphi = 8$, we see that the differences between the NMSE of $N\varphi = 6$ and $N\varphi = 8$ cases at SNR=5 dB are 4.98% and 2.21%, respectively, and at SNR=35dB, these differences are 7.39% and 3.74%, respectively. This means that by reducing the amount of $N\varphi$ from 8 to 6, the accuracy of the classical method reduced twice as much as the proposed method.

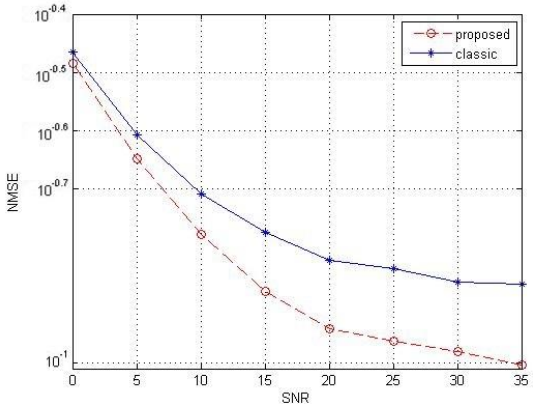

Fig 2. NMSE versus SNR for $Ks = 8$, $N\varphi = 8$.

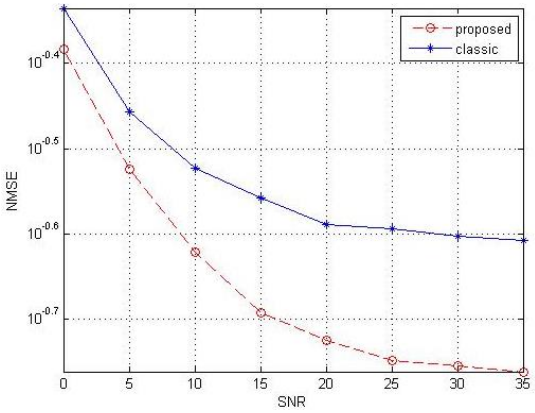

Fig 3. NMSE versus SNR for $Ks=8, N\varphi=6$.

Now, we investigate the results for $Ks=4$. In Fig 4 and Fig 5, similar to the previous figures, the values of $N\varphi$ are 8 and 6, respectively. In Figs. 4 and 5, we considered the lower value of Ks than the previous studies. Although, in general, increasing the amount of Ks improves the quality and decreasing this parameter reduces the quality of the estimated channels; however, this improvement comes at the cost of increasing the size of the problem and the computational complexity. Therefore, we also examined the lower value for Ks (i.e., $Ks=4$). As expected, decreasing the Ks increases the NMSE values in the proposed and classic methods. Now, comparing the results of Fig 4 with Fig 2, we find out that the proposed method has superior performance in this case, too.

Another challenge to consider is the change in the number of users and its impact on the channel estimation process. To obtain this issue, by establishing conditions similar to Fig 2, we increase the user number to 4, which the simulation result is shown in Fig 6. As seen, the result obtained for the classical algorithm is consistent with the result observed in Fig 2. But in the form of the proposed algorithm, we see an accuracy increase. This is due to varying the received paths by increasing the number of users and thus reducing the mutual coherence effect.

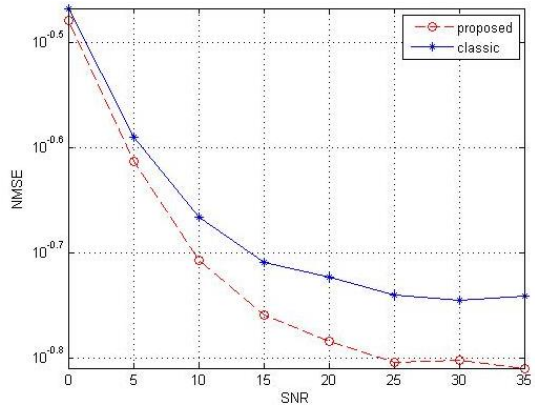

Fig 4. NMSE versus SNR for $Ks=4, N\varphi=8$

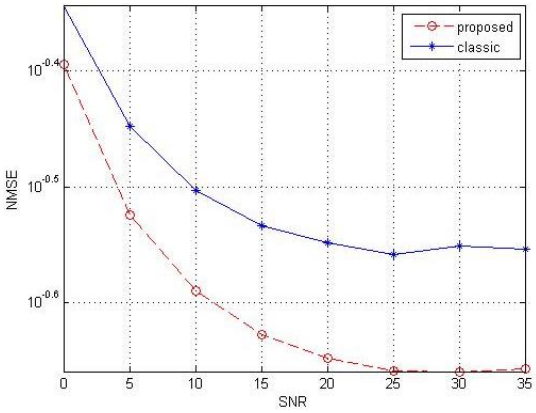

Fig 5. NMSE versus SNR for $Ks=4, N\varphi=6$

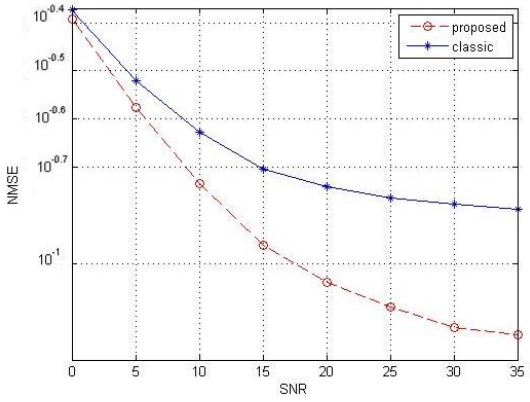

Fig 6. NMSE versus SNR for $Ks=8, N\varphi=8, L=4$.

In the following, we will examine the extent of changes in other parameters and their impact on achieving more desirable quality. Therefore, by assuming SNR=20dB and changing the other parameters, namely N_p (number of panels) and $N\varphi$ (number of pilot symbols), we calculate the NMSE value.

As seen in Fig 7, increasing the N_p reduces the NMSE in both the proposed and the classical algorithms. This is due to the increasing dimension of the measurement matrix, which leads to a higher accurate sparse model solving. Another point regarding the results obtained in Fig 7 is that the proposed algorithm is better than the classical algorithm. Therefore, by increasing the number of panels the higher accurate channel estimation is obtained in the multipanel massive MIMO system. However, the main point is the increase in the costs, which increases with increasing the number of panels. Therefore, to achieve an acceptable accuracy and reasonable implementation costs in a multipanel MIMO system, we need to trade-off between the costs and the estimation accuracy to find the optimal number of panels. In Fig. 8, by assuming SNR=20 dB, we compare the effect of the pilot sequence length changing on the accuracy of channel estimation. As seen, by increasing the $N\varphi$, the NMSE decreases for both methods, which is provided at the cost of reducing the throughput of the system by increasing the pilot overhead. The measurement matrix is a factor in increasing this accuracy. Also, in Fig 8, we see that the proposed method is better than the classical method.

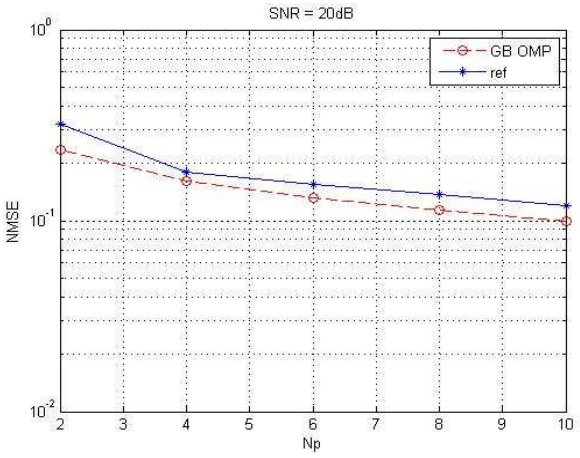

Fig 7. NMSE versus N_p for SNR = 20 dB.

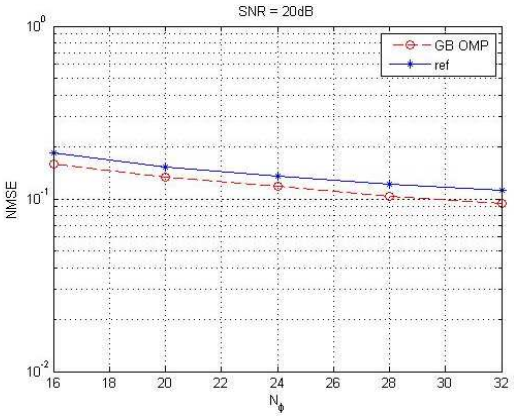

Fig 8. NMSE versus $N\varphi$ for SNR = 20 dB

4.2 | Comparing the methods via BER

In the following, we use the BER criterion to evaluate the quality of channel estimation. In this case, the important point raised in the detection step is the use of the estimated channel matrix instead of the actual channel matrix. For detecting the users' signals, we use the Maximum Likelihood (ML) criterion, in which $\boldsymbol{s}(n)$ is estimated usning the following method:

$$\hat{s}(n) = \underset{\boldsymbol{s}(n)}{argmin}[(\tilde{\boldsymbol{y}}(n) - \boldsymbol{X}_T\boldsymbol{s}(n))^H(\boldsymbol{M}\boldsymbol{M}^H)^{-1}(\tilde{\boldsymbol{y}}(n) - \boldsymbol{X}_T\boldsymbol{s}(n))] \quad (27)$$

In which $\boldsymbol{s}(n)$ is the trasmtted signals vactor that its *l*-th element indicates the 4PSK modulator output signals of the *l*-th user in the *n*-th symbol, $\tilde{\boldsymbol{y}}(n)$ is the received signal vector that its *n*-th element indicates the output signal of n-th pannel's RF chain in the *n*-th symbol, and $\boldsymbol{X}_T = [\boldsymbol{x}_1, \boldsymbol{x}_2, \ldots, \boldsymbol{x}_{N_p}]$ with $\boldsymbol{x}_{n_p} = \boldsymbol{m}_{n_p}^T \widehat{\boldsymbol{H}}_{n_p}$, $\widehat{\boldsymbol{H}}_{n_p} = [\widehat{\boldsymbol{h}}_{n_p,1}, \widehat{\boldsymbol{h}}_{n_p,2}, \ldots, \widehat{\boldsymbol{h}}_{n_p,L}]$.

In the next simulation, we use the estimated channel matrix is obtained by parameters $Ks = 4$, $N\varphi = 8$, and L=2 in (27), and compare the BER versus SNR for uplink transmitting the 2 users' signal. The result that is shown in Fig. 9 indicates that by increasing SNR, the BER decreases, which is as expected. Also, the BER associated with the proposed method is lower than that of the classic method. Since the channel estimation accuracy of the proposed method is better than that of the classic method, the detection accuracy of the proposed method is higher than that of the classic method.

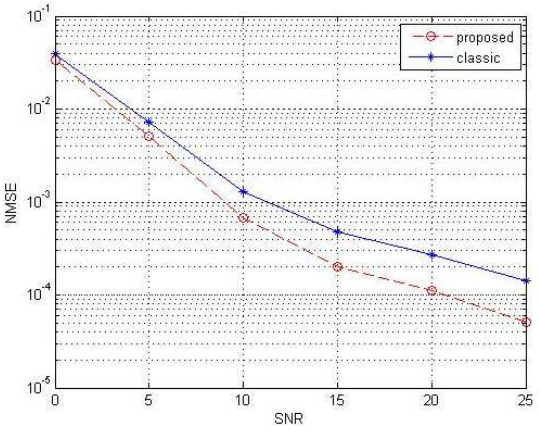

Fig 9. BER versus SNR for $Ks = 4$, $N\varphi = 8$, and L=2

5 | CONCLUSION

In this paper, we proposed a channel estimation method for the millimeter wave multiuser multipanel MIMO systems. In the proposed method the channel estimation problem transformed to an angular domain block sparse signal recovery problem, which was solved by the proposed generalized block OMP method. The accuracy of the proposed method was measured using NMSE and BER criteria, which simulation results indicated the superior performance of the proposed method compared to that of the classic method.

REFERENCES

1. Sh. Dang, O. Amin, B. Shihada, and M. S. Alouini, "What should 6G be?", Nature Electronics, (2020), vol. 3, pp. 20–29.
2. "IEEE Draft Standard for Information Technology - Telecommunications and Information Exchange Between Systems Local and Metropolitan Area Networks -- Specific Requirements - Part 11: Wireless LAN Medium Access Control (MAC) and Physical Layer (PHY) Specifications," in IEEE P802.11-REVmd/D3.0, October 2019 , pp.1-4647, 18, 2019.
3. K. A. Bonsu,, S. Pan., and J. A. Ansere, "Joint user selection and power allocation optimization for energy-efficient MU-MIMO systems with limited feedback" Telecommun Syst 77, 479–492 ,2021.
4. Y. Zhu, H. Guo and V. K. N. Lau, "Bayesian Channel Estimation in Multiuser Massive MIMO With Extremely Large Antenna Array," in IEEE Transactions on Signal Processing, (2021), vol. 69, pp. 5463-5478.
5. Y. -R. Lee, W. -S. Lee, J. -S. Jung, C. -Y. Park, Y. -H. You and H. -K. Song, "Hybrid Beamforming With Reduced RF Chain Based on PZF and PD-NOMA in mmWave Massive MIMO Systems," in IEEE Access, (2021), vol. 9, pp. 60695-60703.
6. P. Jeyakumar., A. Ramesh, and S. Srinitha,, " Wideband hybrid precoding techniques for THz massive MIMO in 6G indoor network deployment.," Telecommun Syst ,2021.
7. J. A. Zhang, S. Member, X. Huang, and S. Member, "Massive Hybrid Antenna Array for Millimeter Wave Cellular Communications," IEEE Commun. Mag., (2015), vol.5, pp.1-18.
8. S. Payami, Hybrid Beamforming for Massive MIMO Systems, Doctor of Philosophy Institute for Communication Systems Faculty of Engineering and Physical

Sciences University of Surrey Guildford, Surrey GU2 7XH, U.K. 2017.

9. L. Zhao, S. Member, D. Wing, K. Ng, and J. Yuan, "Multiuser Precoding and Channel Estimation for Hybrid Millimeter Wave Systems," IEEE J. Sel. Areas Commun., (2017), vol. 35, no. 7, pp. 1576–1590.
10. D. Zhang, S. Member, Y. Wang, Z. Su, W. E. I. Xiang, and S. Member, "Millimeter Wave Channel Estimation Based on Subspace Fitting," IEEE Access, (2018), vol. 6, pp. 76126–76139.
11. S. Wan, H. Zhu, K. Kang and H. Qian, "On the Performance of Fully-Connected and Sub-Connected Hybrid Beamforming System," in IEEE Transactions on Vehicular Technology, (2021), vol. 70, no. 10, pp. 11078-11082.
12. Z. Jiang, P. Chen, F. Yang and Q. Bi, "Experimental Evaluation of A Novel Antenna Structure: Multipanel Massive MIMO," 2018 10th International Conference on Wireless Communications and Signal Processing (WCSP), pp. 1-5, 2018.
13. "Chairmans Notes," 3GPP TSG RAN WG1 NR Ad-Hoc Meeting, Spokane, USA, Jan. 2017
14. Huawei, "R1-1610893: WF on MIMO transmission based on multiple antenna panels", 3GPP TSG RAN WG1 Meeting #86bis, Oct. 2016.
15. N. Song, P. Wen, H. Sun and T. Yang, "Multipanel Based Hybrid Beamforming for Multiuser Massive MIMO," GLOBECOM 2017 - 2017 IEEE Global Communications Conference, pp. 1-6, 2017.
16. N. Amani, H. Wymeersch, U. Johannsen, A. B. Smolders, M. V. Ivashina and R. Maaskant, "Multipanel Sparse Base Station Design With Physical Antenna Effects in Massive MU-MIMO," in IEEE Transactions on Vehicular Technology, (2020), vol. 69, no. 6, pp. 6500-6510.
17. Y. Huang, Y. Li, H. Ren, J. Lu, and W. Zhang, "Multipanel MIMO in 5G," IEEE Commun. Mag., (2018), vol. 56, no. March, pp. 56–61.
18. W. Wang and W. Zhang, "Truncated Tree Based Hybrid Beamforming for Multipanel MIMO," in IEEE Transactions on Vehicular Technology, (2020), vol. 69, no. 11, pp. 13974-13978.
19. B. Hassan, S. Baig, H. M. Asif, S. Mumtaz and S. Muhaidat, "A Survey of FDD-Based Channel Estimation Schemes with Coordinated Multipoint," in IEEE Systems Journal, (2021), Early Access.
20. P. Pasangi, M. Atashbar, and M. Mohassel Feghhi. "Blind downlink channel estimation for TDD-based multiuser massive MIMO in the presence of nonlinear HPA." ETRI Journal, (2019), vol. 41, no. 4, pp. 426-436.
21. M. A and A. P. Kannu, "Channel Estimation Strategies for Multiuser mmWave Systems," in IEEE Transactions on Communications, (2018), vol. 66, no. 11, pp. 5678-5690.
22. W. Wang, W. Zhang, Y. Li, and J. Lu, "Channel Estimation and Hybrid Precoding for Multipanel Millimeter Wave MIMO," 2018 IEEE Int. Conf. Commun., (2018), pp. 1–6.
23. W. Wang and W. Zhang, "Orthogonal Projection Based Channel Estimation for Multipanel Millimeter Wave MIMO," IEEE Trans. Commun., (2020), vol. 68, no. 4, pp. 2173-2187.
24. G. A. F. Seber, "A matrix handbook for statisticians," vol. 15. John Wiley &Sons,75,2008.
25. J. A. Tropp and A. C. Gilbert, "Signal recovery from random measurements via orthogonal matching pursuit," IEEE Trans. Inf. Theory, (2007), vol. 53, no. 12, pp. 4655–4666.
26. N. Shalavi, M. Atashbar, M. Mohassel Feghhi, "Downlink channel estimation of FDD based massive MIMO using spatial partial-common sparsity modeling," Physical Commination, (2020) vol. 42, pp 1-11.